The Astrophysical Journal Supplement Series, 234:15 (13pp), 2018 January https://doi.org/10.3847/1538-4365/aa9f28

Formation and High-order Carboxylic Acids (RCOOH) in Interstellar Analogous Ices of Carbon Dioxide (CO_2) and Methane(CH_4)

Cheng Zhu[1,2], Andrew M. Turner[1,2], Matthew J. Abplanalp[1,2], and Ralf I. Kaiser[1,2]
[1] Department of Chemistry, University of Hawaii at Mânoa, Honolulu, HI 96822, USA; ralfk@hawaii.edu
[2] W.M. Keck Laboratory in Astrochemistry, University of Hawaii at Mânoa, Honolulu, HI 96822, USA
Received 2017 October 10; revised 2017 November 13; accepted 2017 November 30; published 2018 January 16

Abstract

This laboratory study simulated the abiotic formation of carboxylic acids (RCOOH) in interstellar analogous ices of carbon dioxide (CO_2) and methane (CH_4) at 10 K upon exposure to energetic electrons. The chemical processing of the ices and the subsequent warm-up phase were monitored online and in situ, exploiting Fourier Transform Infrared Spectrometry and quadrupole mass spectrometry. Characteristic absorptions of functional groups of carboxylic acids (RCOOH) were observed in the infrared spectra of the irradiated ice. Two proposed reaction mechanisms replicated the kinetic profiles of the carboxylic acids along with the decay profile of the precursors during the irradiation via hydrocarbon formation, followed by carboxylation and/or through acetic acid along with mass growth processes of the alkyl chain. Mass spectra recorded during the warm-up phase demonstrated that these acids are distributed from acetic acid (CH_3COOH) up to decanoic acid ($C_9H_{19}COOH$). High-dose irradiation studies (91 ± 14 eV) converted low-molecular-weight acids such as acetic acid (CH_3COOH) and propionic acid (C_2H_5COOH) to higher-molecular-weight carboxylic acids, compared to low-dose irradiation studies (18 ± 3 eV). The traces of the $H_2C{=}C(OH)_2^+$ ($m/z = 60$) fragment—a link to linear carboxylic acids—implied that higher-order acids ($C_nH_{2n+1}COOH$, $n \geqslant 5$) are likely branched, which correlates with the recent analysis of the structures of the monocarboxylic acids in the Murchison meteorite.

Key words: astrobiology – astrochemistry – cosmic rays – meteorites, meteors, meteoroids – methods: laboratory: solid state

1. Introduction

During the last decade, carboxylic acids (RCOOH)—organic molecules carrying a hydrocarbon group (R) and a carboxyl acid moiety (COOH)—have received considerable attention from the astrochemistry, astronomy, and laboratory astrophysics communities (Bennett & Kaiser 2007; Kim & Kaiser 2010; Shiao et al. 2010; Quirico et al. 2016; Palau et al. 2017; Vinogradoff et al. 2017). This is due to the fact that carboxylic acids are considered crucial biomarkers and potential reaction intermediates for forming amino acids, proteins, and lipids (Ehrenfreund et al. 2001; Georgiou & Deamer 2014; Smith et al. 2015). Formic acid (HCOOH), the simplest carboxylic acid, is the active agent in ant bites, bee stings, and the stinging nettle plant. Acetic acid (CH_3COOH) has an acetyl group ($CH_3C{=}O$) and is a key component of neurotransmitters, acetylcholine, and acetyl-CoA. Long chain carboxylic acids act as backbones of lipids, which perform critical biological functions including storing energy, signaling, and cell membranes.

Currently, only two carboxylic acids—formic acid (HCOOH) and acetic acid (CH_3COOH)—have been identified in the interstellar medium (ISM; Table 1). Formic acid (HCOOH) was first observed in star-forming region Sagittarius B2 (Sgr-B2) at column densities of 10^{12} to 3×10^{15} cm^{-2} via the emission at 18.3 cm (1_{11}–1_{10} transition) using the National Radio Astronomy Observatory (Zuckerman et al. 1971). Acetic acid (CH_3COOH) was first probed toward Sgr-B2 as well (Mehringer et al. 1997). The fractional abundances of formic acid (HCOOH) and acetic acid (CH_3COOH) with respect to molecular hydrogen in Sgr-B2 are about 10^{-9} and $(0.8–6.0) \times 10^{-10}$, respectively (Zuckerman et al. 1971; Liu et al. 2001; Remijan et al. 2002). Since the fractional abundances decrease as the chemical complexity rises, it is reasonable to expect the presence of—hitherto unobserved—more chemically complex carboxylic acids with lower fractional abundances compared to acetic acid in the ISM.

Compared to the ISM, complex carboxylic acids (RCOOH) carrying straight and branched carbon chains have been found in meteorites (Table 1). The first observance of carboxylic acids (RCOOH) in meteorites was reported by Yuen & Kvenvolden (1973). These authors identified 18 monocarboxylic acids with the general molecular formula $C_nH_{2n+1}COOH$ ($n = 2$–8) in the extracts of the Murray and Murchison meteorites. Analyses of Antarctic meteorites revealed more than 35 C_2 to C_{12} monocarboxylic acids (Naraoka et al. 1999). Recently, Huang et al. (2005) re-examined the Murchison and EET96029.20 meteorites and identified more than 50 aliphatic carboxylic acids. They confirmed the indigenous nature of formic acid in these meteorites by its deuterium (D) enrichment. Martins et al. (2006) observed different distributions of carboxylic acids in distinct carbonaceous chondrites and suggested that differing levels of aqueous alteration on the meteorite parent bodies might be responsible for this discrepancy. Benzoic acid (C_6H_5COOH)—the prototype of an aromatic carboxylic acid—was also identified in their extractions from the Murchison and Orgueil meteorites. Furthermore, several carboxylic acid derivatives (Pizzarello et al. 2001, 2004) including nicotinic acid (m–C_5H_4NCOOH, known as vitamin B_3 and niacin) have been detected in a series of carbonaceous chondrites such as the Murchison and Tagish Lake meteorites.

Despite the importance of carboxylic acids in extraterrestrial environments, their detailed formation routes have not yet been resolved. Various gas-phase synthetic routes have been proposed. Irvine et al. (1989) attributed the formation of HCOOH to an unstudied ion-molecule reaction (1) followed by

Table 1
Compilation of Identified Carboxylic Acids in the ISM and in Meteorites

	Species	Source	Reference
Interstellar medium	Formic acid (HCOOH)	Sgr B2	Zuckerman et al. (1971)
		L134N	Irvine et al. (1990)
		W 33A	Schutte et al. (1999)
		e.g., GL 989	Keane et al. (2001)
		Orion KL, Sgr B2, and W51	Liu et al. (2001)
		e.g., OMC-1	Ikeda et al. (2001)
		e.g., AFGL 490	Gibb et al. (2004)
		e.g., MC G	Requena-Torres et al. (2006)
		L1448 and L183	Requena-Torres et al. (2007)
		NGC 1333-IRAS4B and IRAS2A	Bottinelli et al. (2007)
		e.g., AFGL 2591	Bisschop et al. (2007)
		Lynds 1157 B1	Sugimura et al. (2011)
		B1-b	Cernicharo et al. (2012)
		IRAS 20126+4104	Palau et al. (2017)
	Acetic acid (CH_3COOH)	Sgr B2	Mehringer et al. (1997)
		Sgr B2, and W51	Remijan et al. (2002)
		e.g., Orion KL	Remijan et al. (2003)
		e.g., IRAS 16293–2422	Cazaux et al. (2003)
		G19.61-0.23, G29.96–0.02	Shiao et al. (2010)
		e.g., IRAS 16293–2422	Jørgensen et al. (2016)
Meteorite	18 C_2 to C_8 MCA[a]	Murchison and Murray	Yuen & Kvenvolden (1973)
	35 C_2 to C_{12}MCA[a]	Antarctic meteorites	Naraoka et al. (1999)
	7 MCA[a] and 18 DCA[b]	Tagish Lake	Pizzarello et al. (2001)
	11 MCA[a] and 15 DCA[b]	Bells	Monroe & Pizzarello (2011)
	>50 MCA[a]	Murchison	Huang et al. (2005)
	7 MCA[a] and 2 DCA[b]	Orgueil	Martins et al. (2006)

Notes.
[a] MCA = monocarboxylic acids.
[b] DCA = dicarboxylic acids.

a dissociative recombination (Reaction (2)):

$$CH_4 + O_2^+ \rightarrow HCOOH_2^+ + H, \quad (1)$$

$$HCOOH_2^+ + e^- \rightarrow HCOOH + H. \quad (2)$$

Ehrenfreund & Charnley (2000) speculated that protonated methanol can transfer an alkyl cation to formic acid (reaction (3)) followed by a dissociative recombination via reaction (4) to form acetic acid:

$$CH_3OH_2^+ + HCOOH \rightarrow CH_3COOH_2^+ + H_2O, \quad (3)$$

$$CH_3COOH_2^+ + e^- \rightarrow CH_3COOH + H. \quad (4)$$

Nevertheless, later investigations asserted that these reactions would be unfavorable compared to competing channels and indicated that grain surfaces also play a critical role in the formation of carboxylic acids (Garrod & Herbst 2006; Garrod et al. 2008). The authors applied a speculative gas-grain chemical network method to investigate the evolution of complex organic molecules in the warm-up phase of hot molecular cores and suggested successive, unstudied radical reactions (5–9) for the production of formic acid (HCOOH) and acetic acid (CH_3COOH) during the warm-up phase:

$$H_2O \rightarrow H + OH, \quad (5)$$

$$H + CO \rightarrow HCO, \quad (6)$$

$$HCO + OH \rightarrow HCOOH, \quad (7)$$

$$CH_3CHO + CH_3 \rightarrow CH_3CO + CH_4, \quad (8)$$

$$CH_3CO + OH \rightarrow CH_3COOH. \quad (9)$$

Goumans et al. (2008) launched a quantum chemical study of the reaction of hydroxyl radicals (OH) with carbon monoxide (CO) on a carbonaceous surface and implied that the HOCO radical is an important intermediate in the formation of formic acid (HCOOH):

$$OH + CO \rightarrow HOCO, \quad (10)$$

$$HOCO + H \rightarrow HCOOH. \quad (11)$$

In addition to theoretical suggestions and calculations, several laboratory studies untangled the formation routes of carboxylic acids in interstellar analogous ice. Based on kinetic fitting of infrared data, Bennett & Kaiser (2007) revealed that acetic acid (CH_3COOH) can be produced by irradiation of methane (CH_4)–carbon dioxide (CO_2) ice using energetic electrons via the radical–radical recombination of the methyl radical (CH_3) with the hydroxycarbonyl radical (HOCO) at 10 K within the ices. Later, Bennett et al. (2011) exploited the same technique and demonstrated the formation of formic acid (HCOOH) in electron-irradiated water (H_2O)-carbon monoxide (CO) ices through the recombination of the formyl radical (HCO) with the hydroxyl radical (OH) (reaction (7)). Longer carbon-chain carboxylic acids (RCOOH) (Kim & Kaiser 2010) and aromatic carboxylic acids (McMurtry et al. 2016) were identified in alkane (C_nH_{2n+2}; n = 1–6)—carbon dioxide (CO_2) and benzene (C_6H_6)—carbon dioxide (CO_2) ices, respectively, upon exposure to energetic electrons. The formation of carboxylic acids in these experiments was suggested to commence with the cleavage of the carbon–hydrogen bonds

(reactions (12) and (13)) of methane and a generic hydrocarbon, respectively. The released hydrogen atoms have excess kinetic energy of a few electron volts (Bennett et al. 2006) and can overcome the barrier of addition to carbon monoxide (CO) and carbon dioxide (CO_2), forming the formyl radical (HCO) and *trans*-hydroxycarbonyl (HOCO) radical, respectively (reactions (6) and (14)). If the geometry is favorable, barrierless radical–radical recombination processes can lead to the formation of formic acid (7)), acetic acid (15)), and alkyl carboxylic acids (16)). It is important to highlight that these processes could produce carboxylic acids at 10 K throughout the interstellar ices. With respect to higher-order carboxylic acids, Kaiser et al. (1995) identified (partially unsaturated) C_{13} to C_{19} acids in a residue of α particle-irradiated CH_4/O_2 ices. However, no detailed kinetic mechanisms could be extracted in these studies.

$$CH_4 \rightarrow CH_3 + H, \quad (12)$$

$$RH \rightarrow R + H, \quad (13)$$

$$H + CO_2 \rightarrow HOCO, \quad (14)$$

$$HOCO + CH_3 \rightarrow CH_3COOH, \quad (15)$$

$$HOCO + R \rightarrow RCOOH. \quad (16)$$

Here, we demonstrate that high-order carboxylic acids (RCOOH) up to $C_9H_{19}COOH$ can be formed in mixed ices of carbon dioxide (CO_2) and methane (CH_4) exposed to ionizing radiation in the form of energetic electrons mimicking secondary electrons released during galactic cosmic rays penetrating interstellar ices. Carbon dioxide (CO_2) was first detected in the ISM in the Rosette and Cone Nebula (AFGL 890, 961 and 989) (d'Hendecourt & Jourdain de Muizon 1989). Up to now, carbon dioxide has been identified toward multiple sources at levels of up to 40% compared to water in the ices (Boonman et al. 2003; Pontoppidan et al. 2008; Boogert et al. 2015). Methane (CH_4) has also been found to be ubiquitous toward molecular clouds such as NGC 7538 IRS 9 and W33A (Lacy et al. 1991; Öberg et al. 2008) at levels up to 13%. In this study, the distribution of the carboxylic acids (RCOOH) was extracted based on the temperature-programmed desorption (TPD) profiles of their molecular ion currents. The behavior of the tracer of linear acids—the $H_2C = C(OH)_2^+$ ($m/z = 60$) fragment—along with the parent peaks indicates that the majority of the formed high-order acids($C_nH_{2n+1}COOH$, $n = 5$) are branched. To our knowledge, a detailed in situ analysis and quantification of the acids formed in the interstellar analogous ices exposed to ionization radiation has not been conducted so far. In addition, our identification of high-order carboxylic acids (RCOOH) might serve as a starting point for synthesizing lipids and even phospholipids in interstellar analogous ices.

2. Experimental

The experiments were conducted in a contamination-free ultra-high vacuum chamber with a base pressure of 8×10^{-11} Torr, which was rendered using a magnetically suspended turbo molecular pump (Osaka TG420 MCAB) backed by an oil-free scroll pump (Anest Iwata ISP-500). A highly polished silver wafer attached to an oxygen-free high conductivity copper target interfaced with a differentially pumped rotary platform was held in the center of the chamber and cooled by a two-stage closed cycle helium cryostat (CTI-Cryogenics 9600). The temperature of the silver wafer was regulated with a precision of ±0.3 K between 10 and 300 K by a programmable temperature controller. The gas mixture was prepared in a gas-mixing chamber by the sequential addition of 100 mbar of methane (CH_4, Advanced Specialty Gases, 99.999%) and 10 mbar of carbon dioxide (CO_2, Airgas, 99.999%). The premixed gases were then deposited to the silver wafer at 10 K via a precision leak valve and glass capillary array for 15 minutes at a pressure of 2×10^{-7} Torr in the main chamber. The thickness of the ice was determined in situ via laser interferometry (Zhou et al. 2014) with one helium–neon (He–Ne) laser operating at 632.8 nm. The light from the laser was reflected at an angle of 2° relative to the ice surface normal. Considering the ratio of carbon dioxide (CO_2) and methane (CH_4) (1:10; see below) and the refractive indexes of pure carbon dioxide ($n_{CO_2} = 1.27 \pm 0.02$) and methane ($n_{CH_4} = 1.34 \pm 0.04$) ices (Bouilloud et al. 2015), the ice thickness was determined to be 950 ± 20 nm.

The infrared spectra of the ices were recorded using a Nicolet 6700 Fourier Transform Infrared Spectrometry (FTIR) spectrometer in the near-infrared (10,000 to 2000 cm^{-1}) and mid-infrared (6000 to 400 cm^{-1}) ranges with 4 cm^{-1} spectral resolution (Figure 1; assignments of the peaks are compiled in Tables 2–4). Figure 1(a) depicts the mid-infrared spectra of the pristine ices. The vibrational assignments are compiled in Table 2. The relative abundance of carbon dioxide (CO_2) and methane (CH_4) was determined via a modified Beer–Lambert law (Turner et al. 2015) and is compiled in Table 5. The average column density of carbon dioxide (CO_2) was determined as $(1.99 \pm 0.20) \times 10^{17}$ molecules cm^{-2} based on the integrated areas along with absorption coefficients of 1.40×10^{-18} cm $molecule^{-1}$, 4.50×10^{-19} cm $molecule^{-1}$, and 7.80×10^{-17} cm $molecule^{-1}$ for the 3699 cm^{-1} ($\nu_1 + \nu_3$), 3594 cm^{-1} ($2\nu_2 + \nu_3$), and 2274 cm^{-1} (ν_3, $^{13}CO_2$) bands, respectively (Gerakines et al. 1995). The average column density of methane (CH_4) was found to be $(1.91 \pm 0.20) \times 10^{18}$ molecules cm^{-2} based on the integrated areas along with absorption coefficients of 6.85×10^{-19} cm $molecule^{-1}$, 3.59×10^{-19} cm $molecule^{-1}$, and 2.76×10^{-19} cm $molecule^{-1}$ for the 4299 cm^{-1} ($\nu_3 + \nu_4$), 4200 cm^{-1} ($\nu_1 + \nu_4$), and 2813 cm^{-1} ($\nu_2 + \nu_4$) bands, respectively (Brunetto et al. 2008). Therefore, the ratio of carbon dioxide (CO_2) and methane (CH_4) is nominally 1:10, which matches the gas-phase ratio. Taking into account the densities of carbon dioxide (CO_2, 1.6 g cm^{-3}) and methane (CH_4, 0.53 g cm^{-3}) (Wyckoff 1965; Donnay & Ondik 1972), the total thickness of the ice was found to be 1030 ± 100 nm, which is in agreement with the data derived from the laser interferometry method (950 ± 20 nm).

The ices were then isothermally irradiated at 10.0 ± 0.3 K with 5 keV electrons from a Specs Equations (22)–(35) electron gun at nominal beam currents of 0 nA (blank), 1000, and 5000 nA with an extraction efficiency of the electrons of 78.5%. The electrons were introduced at an angle of 15° relative to the target surface and expanded to cover the ice area (3.2 ± 0.3 cm^2). Monte Carlo simulations (Casino 2.42) (Drouin et al. 2007) were exploited to model the electron trajectories and energy transfer inside the ices. The average penetration depth of the 5 keV electrons was calculated to be 692 ± 70 nm, which is less than the thickness of the deposited

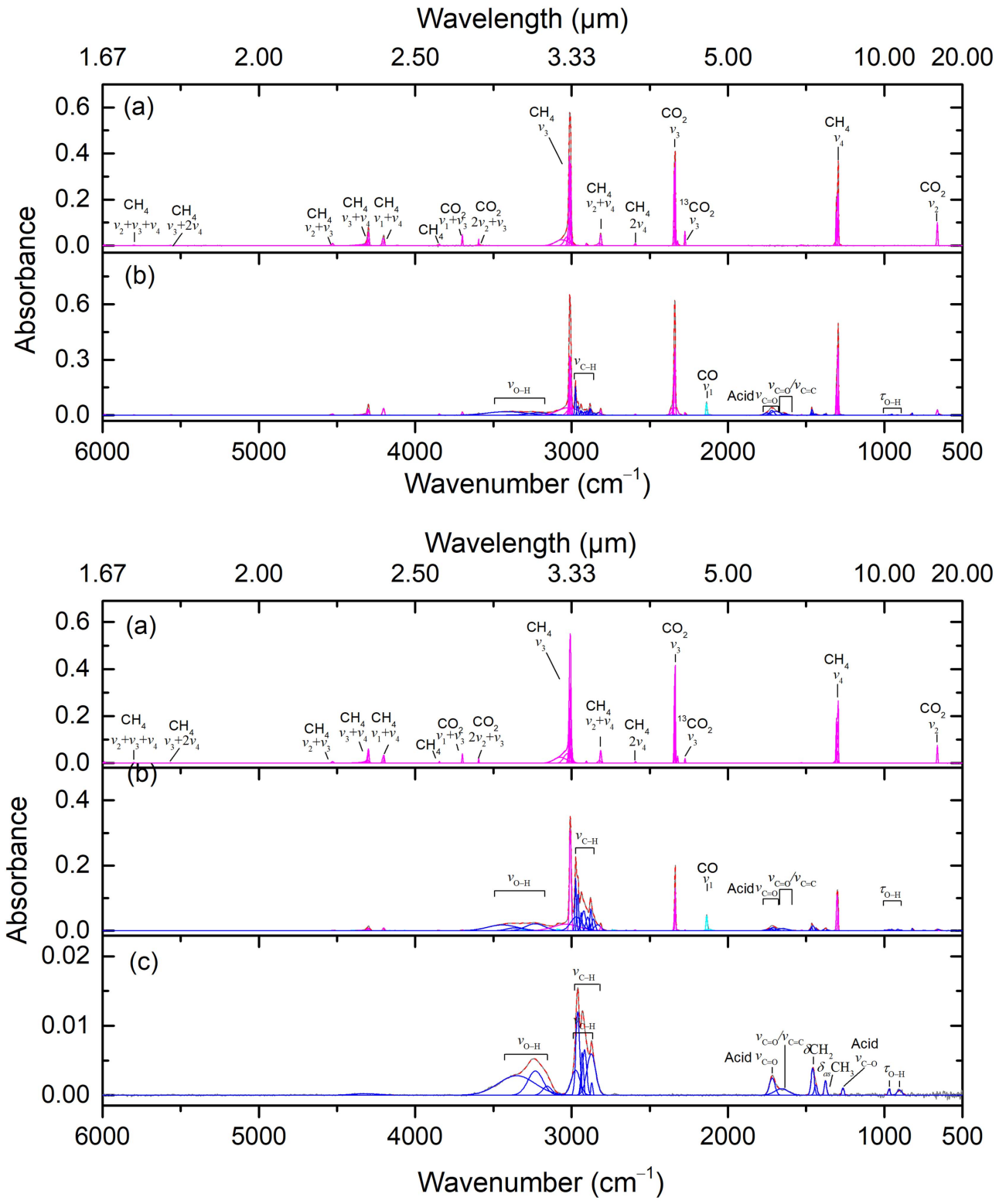

Figure 1. Deconvoluted infrared spectra of carbon dioxide (CO_2) and methane (CH_4) ice for the low-dose (top) and high-dose (bottom) irradiation experiments: (a) pristine ice at 10 K; (b) after irradiation at 10 K; (c) residue at 300 K. Note that no residue was generated in the low-dose experiment.

ice mixtures of 950 ± 20 nm, ensuring negligible interaction between the substrate and the electrons. The averaged doses were found to be 18 ± 3 and 91 ± 14 eV per molecule for nominal beam currents of 1000 and 5000 nA, respectively. The irradiated ices were kept at 10.0 ± 0.3 K for one hour and then warmed up to 300 K at a rate of 1 K minutes^{-1}. In situ FTIR spectra were collected throughout the irradiation and the TPD studies at intervals of 2 minutes. Simultaneously, the mass spectra (mass-to-charge ratio up to 200) of the species in the gas phase were recorded using a Balzer QMG 422 Quadrupole

Table 2
Absorption Peaks Observed in Pristine Carbon Dioxide (CO_2) and Methane (CH_4) Ice

Wavenumber (cm^{-1})	Assignment	Reference
5987	CH_4 ($2\nu_3$)	(1)
5799	CH_4 ($\nu_2 + \nu_3 + \nu_4$)	(1)
5595, 5564	CH_4 ($\nu_3 + 2\nu_4$)	(1)
4957	CO_2 ($\nu_1 + 2\nu_2 + \nu_3$)	(1)
4528	CH_4 ($\nu_2 + \nu_3$)	(1)
4355, 4317, 4305, 4299	CH_4 ($\nu_3 + \nu_4$)	(1)
4205, 4200	CH_4 ($\nu_1 + \nu_4$)	(1)
4115	CH_4 ($\nu_2 + 2\nu_4$)	(1)
3845	CH_4 ($3\nu_4$)	(2)
3699	CO_2 ($\nu_1 + \nu_3$)	(3)
3594	CO_2 ($2\nu_2 + \nu_3$)	(3)
3072, 3028, 3013, 3010, 3007	CH_4 (ν_3)	(2)
2905	CH_4 (ν_1)	(2)
2821, 2813	CH_4 ($\nu_2 + \nu_4$)	(2)
2592	CH_4 ($2\nu_4$)	(2)
2343, 2337, 2323	CO_2 (ν_3)	(3)
2274	$^{13}CO_2$ (ν_3)	(3)
1529	CH_4 (ν_2)	(2)
1307, 1300, 1295	CH_4 (ν_4)	(2)
661	CO_2 (ν_2)	(3)

References. (1) Gerakines et al. (2005), (2) Bennett et al. (2006), (3) Bouilloud et al. (2015).

Mass Spectrometer operating in residual-gas analyzer mode with an electron impact ionization energy of 100 eV and an emission current of 0.7 mA.

3. Results

3.1. Infrared Spectroscopy

3.1.1. Qualitative Analysis

Figure 1(b) displays the infrared spectra of the ices at 10 K after the irradiation. The radiation-induced features are compiled in Table 3. These new absorptions were assigned to functional groups, but not to individual molecules, since the absorptions of the functional groups such as carbonyl (C=O) are not unique for individual molecules (Abplanalp et al. 2016a). The formation of carboxylic acids (RCOOH) in irradiated ices at 10 K was evidenced by the characteristic absorptions of carbonyl (C=O) and hydroxyl (O–H) groups at 1750–1720 and 3600–2500 cm^{-1}, respectively. These two absorptions are complicated by the presence of both ketones (R_2CO)/aldehydes (RCHO) and alcohols (ROH) in the irradiated ices, respectively. However, the characteristic bands of alcohols in the range of 1100–1000 cm^{-1} (C–O) (McDonald et al. 1996) were unidentifiable in the spectra, which indicates that alcohols were not effectively formed upon irradiation. Sander & Gantenberg (2005) reported that the aggregation of acetic acid (CH_3COOH) and propionic acid (CH_3CH_2COOH) in argon (Ar) matrices shifts the band of C=O stretch from about 1780 $cm^{-1}$to about 1720 cm^{-1} and transforms the band of O–H stretch from about 3570 cm^{-1} to a multi-band pattern ranging from 3200 to 2500 cm^{-1}, which agrees quite well with our studies. The observation of the bands at about 1270 cm^{-1} (C=O stretch) and 970–875 cm^{-1} (O–H out-of-plane deformation) (Socrates 2004) further supports the identification of carboxylic acids.

Figure 1(c) depicts the spectrum of the residue recorded at 300 K after the high-dose irradiated ice was warmed up. The precursors carbon dioxide (CO_2) and methane (CH_4), as well as irradiation-induced low-sublimation temperature compounds, sublimed during the warm-up phase. The dominant components of the residue were higher-order carboxylic acids (RCOOH). Here, their typical peaks were identified as: O–H stretch in the 3600–3000 cm^{-1} range, C=O stretch at 1717 cm^{-1}, C–O stretch at 1264 cm^{-1}, and O–H out-of-plane deformation at 969 and 903 cm^{-1} (Table 4). The CH_3/CH_2 group stretches at 2973, 2961, 2932, 2917, 2874, and 2871 cm^{-1}, along with deformations at 1458, 1438, and 1376 cm^{-1}, further corroborated the alkyl functionality of carboxylic acids (RCOOH). No residue was observed on the silver wafer at 300 K in the case of the 1000 nA irradiation, which indicates the carbon chain of the carboxylic acids (RCOOH) produced in the low-dose experiment is much shorter than those produced in the high-dose irradiation.

3.1.2. Quantitative Analysis

Figure 2 compiles the temporal development of the column density of carbon dioxide (CO_2), methane (CH_4), carbon monoxide (CO), and carboxylic acids (RCOOH) during the irradiation. As mentioned above, the average column densities of carbon dioxide ($[CO_2]_t$) and methane ($[CH_4]_t$) were determined based on the integrated areas along with absorption coefficients for the 3699 cm^{-1} (CO_2, $\nu_1 + \nu_3$), 3594 cm^{-1} (CO_2, $2\nu_2 + \nu_3$), 2274 cm^{-1} ($^{13}CO_2$, ν_3), 4299 cm^{-1} (CH_4, $\nu_3 + \nu_4$), 4200 cm^{-1} (CH_4, $\nu_1 + \nu_4$), and 2813 cm^{-1} (CH_4, $\nu_2 + \nu_4$) bands. The reported absorption coefficient 1.10×10^{-17} cm $molecule^{-1}$ of the 2136 cm^{-1} (ν_1) band was used to evaluate the production of carbon monoxide ($[CO]_t$) (Jamieson et al. 2006). The formation of *trans*-hydrocarboxyl radical (HOCO) was monitored via ν_3 at 1846 cm^{-1} and has an absorption coefficient of 3.60×10^{-17} cm $molecule^{-1}$ (Bennett & Kaiser 2007). The temporal profile of the upper limit of the column densities of the carboxylic acids ($[RCOOH]_t$) was derived based on the mass balance principle:

$$[\mathrm{RCOOH}]_t \leqslant \frac{A_{1720}}{A_{1720} + A_{1640}}([\mathrm{CO_2}]_0 - [\mathrm{CO_2}]_t - [\mathrm{CO}]_t - [\mathrm{HOCO}]_t). \quad (17)$$

Here, A_{1720} and A_{1640} are the integrated areas of the deconvoluted peaks in the C=O stretch region near 1720 and 1640 cm^{-1}, respectively (Kim & Kaiser 2010). These coefficients are used to correct the upper limit of the column densities of the carboxylic acids since the peaks at around 1640 cm^{-1} were attributed to other species containing the C=O/C=C group, but not carboxylic acids. Therefore, the column densities of CO_2, CO, and *trans*-HOCO at the end of 5000 nA irradiation were calculated to be $(2.18 \pm 0.39) \times 10^{16}$, $(5.57 \pm 0.56) \times 10^{16}$, and $(6.97 \pm 0.70) \times 10^{13}$ molecules cm^{-2}, respectively (Table 5). Hence, the upper limit of the radiation-induced carboxylic acids (RCOOH) is $(8.96 \pm 0.26) \times 10^{16}$ molecules cm^{-2}, which returns a yield of about 45% given the original column density of carbon dioxide $[CO_2]_0 = (1.99 \pm 0.20) \times 10^{17}$ molecules cm^{-2}. The column density of high-order carboxylic acids (RCOOH) formed in the low-dose experiment decreased to $(6.53 \pm 0.66) \times 10^{16}$ molecules cm^{-2}, corresponding to a yield of about 33%. This translates into $(5.5 \pm 1.3) \times 10^{-3}$

Table 3
New Absorption Peaks Observed in Carbon Dioxide (CO_2) and Methane (CH_4) Ice after the Irradiation at 10 K

Wavenumber (cm^{-1})		Assignment	Reference
1000 nA	5000 nA		
3418, 3372, 3215	3441, 3359, 3233	O–H stretch (acid)	(1)
3257	3309, 3241	C–H stretch (–C≡CH)	(1)
3094	3092, 3079, 3066	C–H stretch (=CH_2)	(1)
2975, 2961	2974, 2970, 2960	–CH_3 asymmetric stretch	(1)
2941, 2935	2939, 2921	–CH_2–asymmetric stretch	(1)
2916, 2902, 2880	2897, 2882	–CH_3 asymmetric stretch	(1)
2856, 2824	2877, 2861, 2833	–CH_2–sym. stretch	(1)
2741, 2734	2740, 2731, 2718	C–H stretch (O=C–H)	(1)
2651	2651	O–H stretch (acid)	(1)
2137, 2129, 2128	2136, 2128, 2121	CO (ν_1)	(2)
	1955	C=C=C stretch (e.g., H_2C=C=CHR)	(3)
	1846	C=O stretch (*trans*–HOCO radical)	(2)
1751, 1719, 1695	1753, 1721, 1712	C=O stretch (acid)	(1)
1645, 1635	1653, 1644	C=O/C=C stretch	(1)
1464, 1463	1465, 1457	–CH_2–scissor	(1)
1451, 1438	1436, 1425	CH_3 asymmetric deformation	(1)
1378, 1372	1376, 1372, 1353	CH_3 symmetric deformation	(1)
1271	1270, 1262	C–O stretch (acid)	(1)
994, 968, 952, 936, 913	995, 969, 952, 937, 913, 892	O–H out-of-plane deformation (acid)	(1)
821	821	C_2H_6 (ν_{11})	(4)
749, 745	749, 738	C–C skeletal vibration (–$(CH_2)_n$–)	(1)
650	652	C=O bend (acid)	(5)

References. (1) Socrates (2004), (2) Bennett & Kaiser (2007), (3) Kaiser & Roessler (1998), (4) Gerakines et al. (1996), (5) Kim & Kaiser (2010).

Table 4
Absorption Peaks Observed in the Residue of Carbon Dioxide (CO_2) and Methane (CH_4) Ice at 300 K

Wavenumber (cm^{-1})	Assignment	Reference
3351, 3231, 3156	O–H stretch (acid)	(1)
2973, 2961	–CH_3 asymmetric stretch	(1)
2932, 2917	–CH_2–asymmetric stretch	(1)
2874, 2871	–CH_2–symmetric stretch	(1)
1717	C=O stretch (acid)	(1)
1657	C=O/C=C stretch	(1)
1458	–CH_2–scissor (acid)	(1)
1438	–CH_3 asymmetric deformation (acid)	(1)
1376	–CH_3 symmetric deformation (acid)	(1)
1264	C–O stretch (acid)	(1)
969, 903	O–H out-of-plane deformation (acid)	(1)

Reference. (1) Socrates (2004).

carboxylic acids eV^{-1} and $(1.5 \pm 0.3) \times 10^{-3}$ carboxylic acids eV^{-1} for the low-dose and high-dose experiments, respectively. The destroyed methane (CH_4) molecules at 1000 and 5000 nA were found to be $(5.50 \pm 0.77) \times 10^{17}$ and $(1.44 \pm 0.21) \times 10^{18}$ molecules cm^{-2}, respectively (Table 5). These values are about 8 and 16 times the column densities of the carboxylic acids (RCOOH) formed in the corresponding experiments. The higher value for the 5000 nA experiment indicates that the alkyl group of the acids is likely larger than those formed at low doses (1000 nA), provided that all of the destroyed methane (CH_4) was converted to carboxylic acid (RCOOH). This finding is consistent with the fact that residues in the form of higher-order carboxylic acids were observed in the 5000 nA study, but not at a lower dose.

3.2. Mass Spectrometry

In addition to the in situ infrared analysis, the molecules subliming into the gas phase were monitored utilizing a quadrupole mass spectrometer during the irradiation and the warm-up phases. No newly formed compounds were detected in the gas phase except a trace of molecular hydrogen ($m/z = 2$; H_2^+) during the irradiation. Figure 3 depicts the ion currents of methane ($m/z = 16$; CH_4^+) and carbon dioxide ($m/z = 44$; CO_2^+) during the warm-up of the ices irradiated at currents of (a) 0 nA (blank, control experiment), (b) 1000 nA, and (c) 5000 nA. The characteristic fragment ion $COOH^+$ ($m/z = 45$) was used to trace the carboxylic acids (RCOOH) desorbed to the gas phase upon heating (Bennett & Kaiser 2007). The ion currents of $m/z = 45$ below 150 K can be attributed to the natural ^{13}C isotope of carbon dioxide ($^{13}CO_2$) based on a comparison with the trace of $m/z = 44$ ($^{12}CO_2^+$). The ion profile of the $m/z = 45$ peak above 150 K in Figures 3(b) and (c) undoubtedly indicates that carboxylic acids (RCOOH) were produced upon irradiation. Compared to 1000 nA, the irradiation at 5000 nA broadens and shifts this signal to a higher temperature, which indicates that higher-order carboxylic acids were formed at the elevated dose. This observation is consistent with the infrared results (Section 3.1). In addition, the ion current of the $H_2C{=}C(OH)_2^+$ ($m/z = 60$) and $CH_2CH_2COOH^+$ ($m/z = 73$) fragments corroborated the sublimation of carboxylic acids (RCOOH). The $H_2C{=}C(OH)_2^+$ ($m/z = 60$) fragment is a characteristic fragment of carboxylic acids ($C_nH_{2n+1}COOH$, $n = 3$) with a γ-hydrogen—the hydrogen on the third carbon that attaches to the carboxyl group—due to McLafferty rearrangement (McLafferty 1959; Gross 2004). It can serve as a tracer of *linear* acids since for carboxylic acids without a γ-hydrogen, the carbon chain of acids must be highly branched. Note that the molecular ion

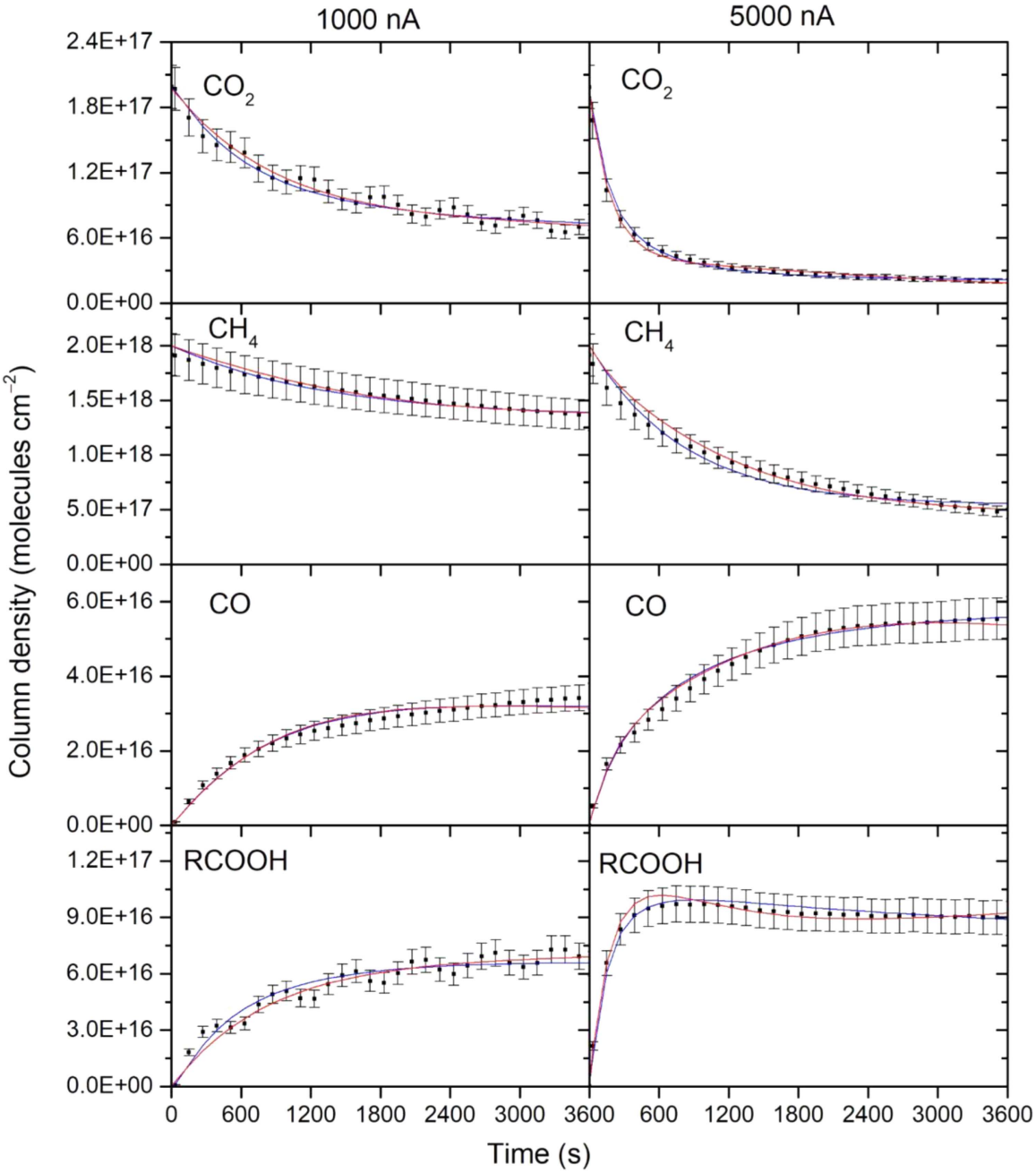

Figure 2. Temporal profiles of the column densities during the low-dose (1000 nA) and high-dose (5000 nA) irradiation at 10 K for carbon dioxide (CO_2), methane (CH_4), carbon monoxide (CO), and the carboxylic acids (RCOOH). The kinetic fits are shown for each species, accounting for the reaction schemes A (red) and B (blue) as compiled in Figure 5.

CH_3COOH^+ partly contributes to the $m/z = 60$ signal (Bennett & Kaiser 2007).

In addition to the characteristic fragments of carboxylic acids (RCOOH), their molecular ions ($C_nH_{2n+1}COOH$, n = 1–9) were also observed during TPD of the irradiated ices (Figure 4). As seen in Figure 4, higher molecular weights for the carboxylic acid are formed as the dose increases. Furthermore, the sublimation onsets increase with the size of the alkyl group of the carboxylic acids (RCOOH): 120 K (CH_3COOH, $m/z = 60$, Figure 3), 125 K ($C_2H_5COOH^+$, $m/z = 74$), 137 K ($C_3H_7COOH^+$, $m/z = 88$), 153 K ($C_4H_9COOH^+$, $m/z = 102$), 169 K ($C_5H_{11}COOH$, $m/z = 116$), 176 K ($C_6H_{13}COOH$, $m/z = 130$), 190 K ($C_7H_{15}COOH$, $m/z = 144$), 196 K ($C_8H_{17}COOH$, $m/z = 158$), and 213 K ($C_9H_{19}COOH$, $m/z = 172$), i.e., an average increase of 5–17 K per additional CH_2 group. This finding is in line with previous studies of alkanes and alkenes in methane (5–16 K) (Jones & Kaiser 2013), ethane (6–16 K) (Abplanalp & Kaiser 2016), and ethylene (3–19 K) (Abplanalp & Kaiser 2017) systems radiolyzed at 5–10 K. Since the carboxylic acids (RCOOH) are complex mixtures and are not well separated in the TPD profiles, it is improbable to elucidate their structural diversity based on the fragment signal. The high-order acids ($C_nH_{2n+1}COOH$, $n \geqslant 5$) are likely branched since the signal of the tracer of linear acids—$m/z = 60$—almost disappears during their sublimation.

A quantification of the sublimed higher-order carboxylic acids (RCOOH) was conducted via evaluating the branching ratio of each acid, deriving the absolute column density of

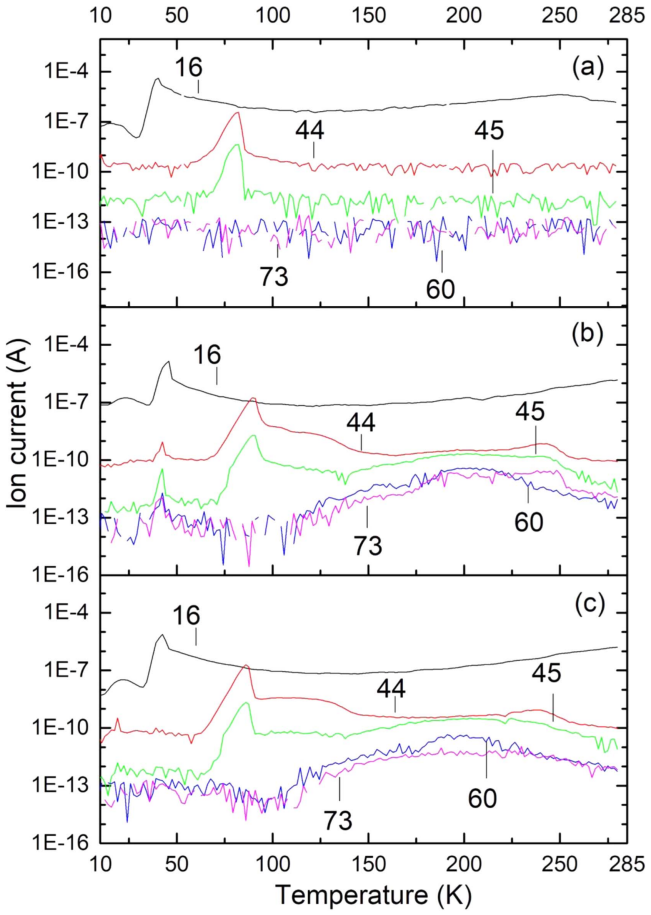

Figure 3. Temporal evolution of the ion currents associated with methane (CH_4^+; $m/z = 16$) and the carbon dioxide (CO_2^+; $m/z = 44$) released during the warm-up phases after (a) 0 nA, (b) 1000 nA, and (c) 5000 nA irradiation of the ice mixtures at 10 K. Note that the ion current of $m/z = 45$ traces the natural abundance of carbon dioxide ($^{13}CO_2$) below 150 K and of the mass fragment ($COOH^+$) of carboxylic acids (RCOOH) at higher temperatures. The ion currents of $m/z = 60$ and $m/z = 73$ trace $H_2C{=}C(OH)_2^+/CH_3COOH^+$ and $CH_2CH_2COOH^+$, respectively.

acetic acid (CH_3COOH) via infrared spectroscopy, and utilizing this concentration to derive column densities of the higher carboxylic acids. The branching ratios of the acids were calculated based on their ionization cross section and integrated area of the molecular ion signal of each acid. The ionization cross section σ_{ion} were determined using the following formula with ±20% uncertainty (Center & Mandl 1972; Kaiser & Suits 1995):

$$\sigma_{ion} = 36(\alpha)^{0.5} - 18. \quad (18)$$

Here, α represents the molecular polarizability, which is calculated as the sum of atomic polarizabilities. Table 6 lists the relative ionization cross section of each acid with respect to acetic acid (CH_3COOH). Since not only acetic acid (CH_3COOH), but also the $H_2C{=}C(OH)_2^+$ fragment contribute to the $m/z = 60$ signal, its profile was deconvoluted (Figure 5 (a)). Peak 1 in the 120–190 K range was assigned to acetic acid (CH_3COOH). This temperature range matches quite well with previous investigations (Bertin et al. 2011; Burke et al. 2015). Peaks 2 and 3 were attributed to the $H_2C{=}C(OH)_2^+$ fragment. The other molecular ion profiles were directly integrated for the corresponding acids. The branching ratios

Table 5
Column Densities of the Identified Species in Carbon Dioxide (CO_2) and Methane (CH_4) Ice before and after the Irradiation at 10 K

	Species	Column Density (molecules cm^{-2})	
		1000 nA	5000 nA
Before irradiation	CO_2	$(1.99 \pm 0.20) \times 10^{17}$	$(1.99 \pm 0.20) \times 10^{17}$
	CH_4	$(1.91 \pm 0.20) \times 10^{18}$	$(1.91 \pm 0.20) \times 10^{18}$
After irradiation	CO_2	$(0.75 \pm 0.08) \times 10^{17}$	$(0.22 \pm 0.04) \times 10^{17}$
	CH_4	$(1.36 \pm 0.14) \times 10^{18}$	$(0.47 \pm 0.05) \times 10^{18}$
	RCOOH[a]	$(6.53 \pm 0.66) \times 10^{16}$	$(8.96 \pm 0.91) \times 10^{16}$
	CO	$(3.46 \pm 0.35) \times 10^{16}$	$(5.57 \pm 0.56) \times 10^{16}$
	HOCO	…	$(6.97 \pm 0.70) \times 10^{13}$
$C_{CH_4 \rightarrow RCOOH}$[b]		$(5.50 \pm 0.77) \times 10^{17}$	$(1.44 \pm 0.21) \times 10^{18}$
$C_{CH_4 \rightarrow RCOOH}/C_{RCOOH}$[c]		8.4 ± 1.9	16.1 ± 3.1

Notes.
[a] The column density of carboxylic acid (RCOOH) was calculated using formula (17); see Section 3.1.2.
[b] $C_{CH_4 \rightarrow RCOOH}$ = column density of destroyed methane (CH_4).
[c] C_{RCOOH} = column density of carboxylic acid (RCOOH).

of the carboxylic acids are compiled in Table 6 and plotted in Figure 6. Low-molecular-weight acids—acetic acid (CH_3COOH), propionic acid (C_2H_5COOH), and butyric acid (C_3H_7COOH)—dominate the products, with propionic acid (C_2H_5COOH) being the most abundant species. These three acids account for (85.6 ± 11.8)% and (77.6 ± 10.9)% of the total acids in the low-dose and high-dose radiationcases, respectively. Starting from valeric acid (C_4H_9COOH), the ratio of each acid formed in the experiment of high-dose radiation turns out to be more than the corresponding acid formed in the low-dose case. It is interesting that increasing the radiation dose converts low-molecular-weight acids such as acetic acid (CH_3COOH) and propionic acid (C_2H_5COOH) to higher-molecular-weight carboxylic acids rather than decomposes/recycles large acids into small molecules. Second, the absolute amount of acetic acid (CH_3COOH) was calculated using the TPD curves of the IR band at 1720 cm^{-1} for the C=O stretch (Figure 5(b)). Combining these results and the TPD profile of the molecular ion signal of the acids, we calculated the amount of the total acids sublimed at multiple temperatures and subsequently obtained the carboxylic acids remaining on the wafer (red squares in Figure 5(b)), and found that the trend is consistent with the infrared observations. At the end of the warm-up phase, the total sublimed acids calculated from the ion signals were found to be $(5.85 \pm 0.61) \times 10^{16}$ and $(4.93 \pm 0.49) \times 10^{16}$ molecules cm^{-2} for 1000 nA and 5000 nA irradiation experiments, respectively. This agrees nicely with the derived values ($(6.53 \pm 0.66) \times 10^{16}$ and $(6.03 \pm 0.61) \times 10^{16}$ molecules cm^{-2}) from the IR spectra (Table 6).

4. Discussion

Having assigned the carriers of the newly formed infrared bands within the irradiated (CO_2) and methane (CH_4) ices, we now attempt to elucidate the reaction mechanism involved in the production of the identified irradiation-induced species. Two reaction schemes, A and B (Figure 7), were derived to

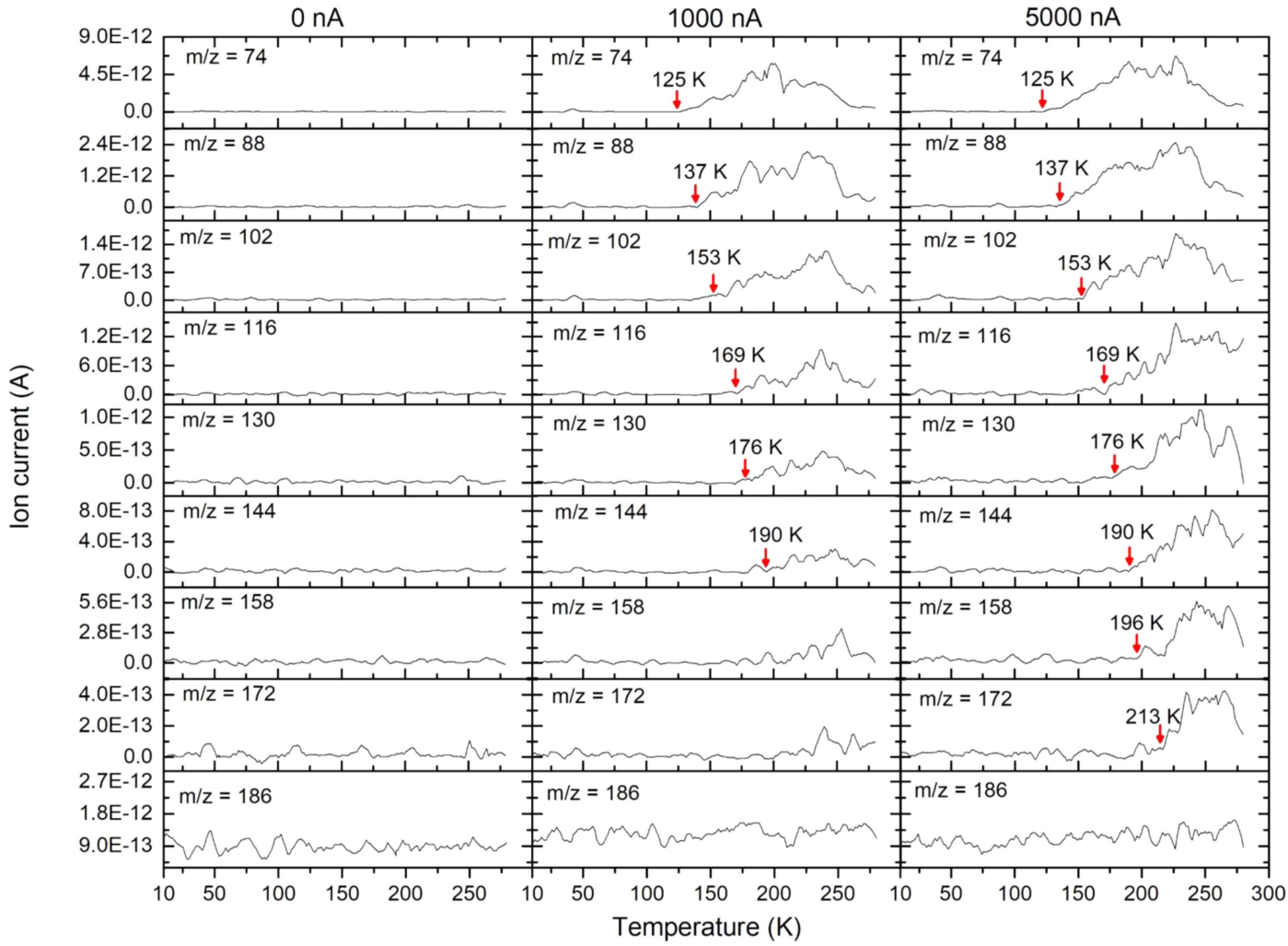

Figure 4. TPD profiles recorded via QMS for $m/z = 74$, 88, 102, 116, 130, 144, 158, 172, and 186, which are associated with carboxylic acids C_2H_5COOH, C_3H_7COOH, C_4H_9COOH, $C_5H_{11}COOH$, $C_6H_{13}COOH$, $C_7H_{15}COOH$, $C_8H_{17}COOH$, $C_9H_{19}COOH$, and $C_{10}H_{21}COOH$, respectively.

Table 6
Calculated Column Densities and Branching Ratios of the Sublimed Carboxylic Acids (RCOOH)

Acid	Ionization Cross Section Relative to CH_3COOH	Column Density (Molecules cm^{-2})		Branching Ratio (%)	
		1000 nA	5000 nA	1000 nA	5000 nA
CH_3COOH	1	$(1.31 \pm 0.25) \times 10^{16}$	$(8.30 \pm 1.58) \times 10^{15}$	22.4 ± 4.9	16.8 ± 3.6
C_2H_5COOH	1.19 ± 0.34	$(2.74 \pm 0.52) \times 10^{16}$	$(2.24 \pm 0.43) \times 10^{16}$	46.8 ± 10.2	45.3 ± 9.7
C_3H_7COOH	1.36 ± 0.38	$(9.53 \pm 1.81) \times 10^{15}$	$(7.60 \pm 1.44) \times 10^{15}$	16.3 ± 3.5	15.4 ± 3.3
C_4H_9COOH	1.50 ± 0.43	$(4.31 \pm 0.82) \times 10^{15}$	$(4.00 \pm 0.76) \times 10^{15}$	7.4 ± 1.6	8.1 ± 1.7
$C_5H_{11}COOH$	1.64 ± 0.46	$(2.14 \pm 0.41) \times 10^{15}$	$(2.92 \pm 0.55) \times 10^{15}$	3.7 ± 0.8	5.9 ± 1.3
$C_6H_{13}COOH$	1.77 ± 0.50	$(1.17 \pm 0.22) \times 10^{15}$	$(1.80 \pm 0.34) \times 10^{15}$	2.0 ± 0.4	3.6 ± 0.8
$C_7H_{15}COOH$	1.88 ± 0.53	$(6.16 \pm 1.17) \times 10^{14}$	$(1.12 \pm 0.21) \times 10^{15}$	1.1 ± 0.2	2.3 ± 0.5
$C_8H_{17}COOH$	1.99 ± 0.56	$(1.32 \pm 0.25) \times 10^{14}$	$(7.27 \pm 0.14) \times 10^{15}$	0.2 ± 0.1	1.5 ± 0.3
$C_9H_{19}COOH$	2.10 ± 0.59	$(8.38 \pm 1.59) \times 10^{13}$	$(5.05 \pm 0.96) \times 10^{14}$	0.1 ± 0.1	1.1 ± 0.2
Total		$(5.85 \pm 0.61) \times 10^{16}$	$(4.93 \pm 0.49) \times 10^{16}$	100.0 ± 12.0	100.0 ± 11.1
Sublimed acid (calculated from IR spectra)		$(6.53 \pm 0.66) \times 10^{16}$	$(6.03 \pm 0.61) \times 10^{16}$		

kinetically fit the temporal evolution of the column densities of carboxylic acids (RCOOH) and its precursors during the irradiation of our samples (Figure 2). The rate constants of each reaction in the schemes were derived by solving seven (scheme A) or eleven (scheme B) coupled differential equations (Frenklach et al. 1992) and compiled in Table 7. These schemes effectively probe if carboxylic acids are formed via conversion of methane to higher hydrocarbons followed by carboxylation (scheme A) or through acetic acid followed by mass growth processes at the alkyl chain (scheme B).

We first describe the reactions in Scheme A. It is well known that radiolysis of methane (CH_4) can produce high-order hydrocarbons (RH; Kaiser & Roessler 1998; Bennett et al. 2006). They can be formed through a successive insertion

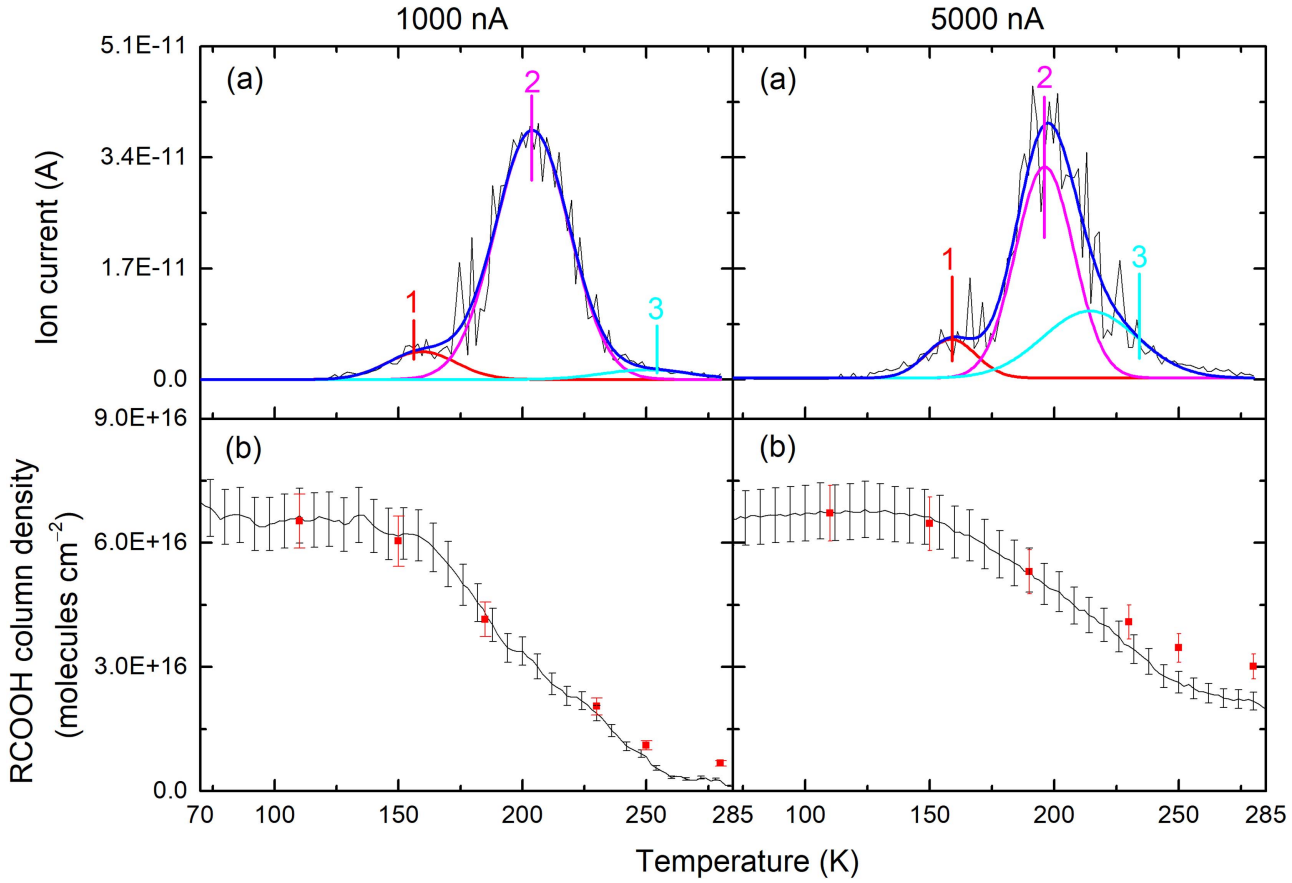

Figure 5. TPD profiles for: (a) $m/z = 60$ and (b) RCOOH column density (From the IR data) recorded in the low-dose (left) and high-dose (right) irradiation experiments. Peak 1 is attributed to CH_3COOH^+. Peaks 2 and 3 are attributed to $H_2C{=}C(OH)_2^+$. The red squares represent RCOOH column density calculated from the QMS data.

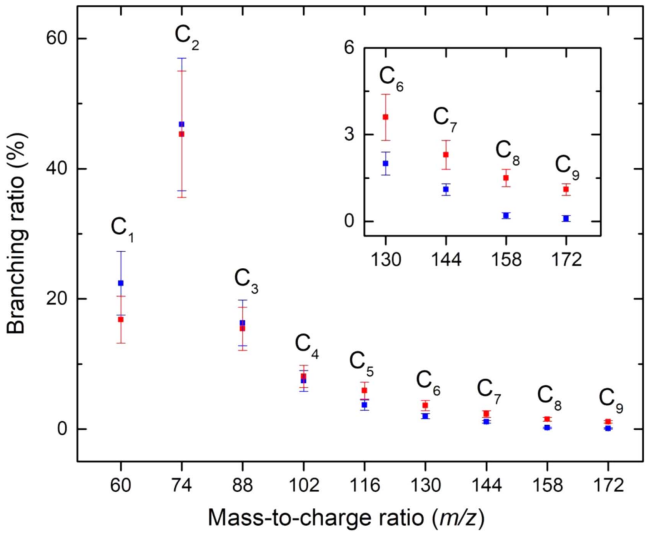

Figure 6. Branching ratios of the sublimed acids ($C_nH_{2n-1}COOH$, $n = 1$–9) formed upon low-dose (blue square) and high-dose irradiation (red square).

of suprathermal carbene, CH_2, into aliphatic C–H bonds:

$$CH_4 \rightarrow CH_2(a^1A_1) + H_2, \quad (19)$$

$$CH_4 + CH_2(a^1A_1) \rightarrow C_2H_6, \quad (20)$$

$$C_2H_6 + CH_2(a^1A_1) \rightarrow C_3H_8, \quad (21)$$

$$C_3H_8 + CH_2(a^1A_1) \rightarrow i/n\text{–}C_4H_{10}. \quad (22)$$

Reaction (19) is endoergic by 483.4 kJ mol^{-1} (5.01 eV) (Mebel et al. 1997). The energies required to complete this process are provided by the energy transferred from the energetic electrons passing through the ices. In addition, radical–radical combination may also contribute to the formation of hydrocarbons (RH) as follows:

$$CH_3 + CH_3 \rightarrow [C_2H_6]^*, \quad (23)$$

$$C_2H_6 \rightarrow C_2H_5 + H, \quad (24)$$

$$C_2H_5 + CH_3 \rightarrow C_3H_8, \quad (25)$$

$$C_2H_5 + C_2H_5 \rightarrow n\text{–}C_4H_{10}. \quad (26)$$

The methyl (CH_3) and ethyl (C_2H_5) radicals can be produced by the cleavage of a carbon–hydrogen bond of methane (CH_4) (reaction (12), Section 1) and ethane (C_2H_6) (reaction (24)), which were calculated to be endoergic by 427.5 kJ mol^{-1} (4.43 eV) and 411.7 kJ mol^{-1} (4.27 eV), respectively (Bennett et al. 2006). The radical–radical combination reactions (23), (25), and (26) are exoergic by 360.7 kJ mol^{-1} (3.74 eV), 369.4 kJ mol^{-1} (3.83 eV), and 363.6 kJ mol^{-1} (3.77 eV), respectively (Pittam & Pilcher 1972; Tsang 1996; Kim et al. 2010; Abplanalp & Kaiser 2016). The hydrocarbons (RH) can react with carbon dioxide (CO_2), leading to the formation of carboxylic acids (RCOOH) via reactions (13), (14), and (16) (Section 1). The released hydrogen atoms from reaction (13) could possess up to a

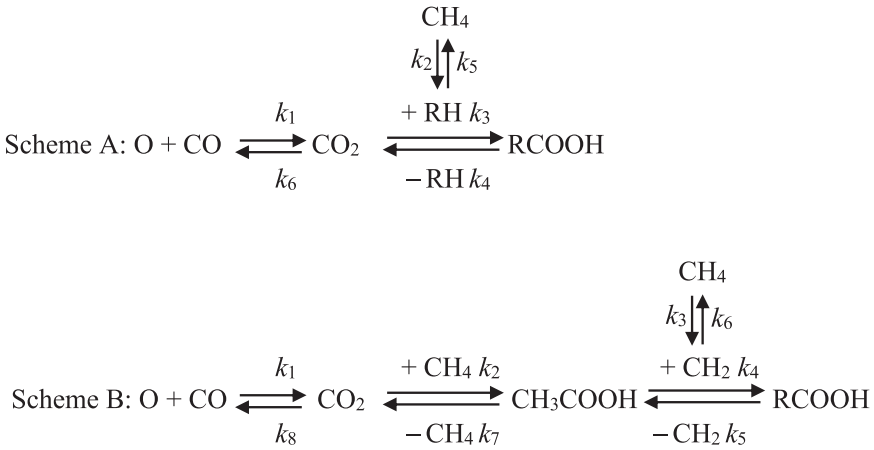

Figure 7. Reaction schemes A and B exploited to fit temporal profiles of the species produced during radiation exposure of carbon dioxide (CO_2) and methane (CH_4) ice at 10 K (Figure 3).

Table 7
Rate Constants Derived via Iterative Solution of Reaction Schemes A and B

Reaction		Rate Constant	
		1000 nA	5000 nA
Scheme A			
$CO_2 \rightarrow CO + O$	k_1[a]	1.92×10^{-4}	6.41×10^{-4}
$CH_4 \rightarrow RH$[b]	k_2[a]	2.33×10^{-4}	8.71×10^{-4}
$CO_2 + RH \rightarrow RCOOH$	k_3[c]	3.26×10^{-20}	3.12×10^{-19}
$RCOOH \rightarrow CO_2 + RH$	k_4[a]	1.90×10^{-2}	1.00×10^{-1}
$RH \rightarrow CH_4$	k_5[a]	5.68×10^{-4}	3.51×10^{-4}
$CO + O \rightarrow CO_2$	k_6[c]	1.44×10^{-20}	4.01×10^{-21}
$CO_2 + CH_4 \rightarrow X$	k_7[c]	4.51×10^{-23}	2.06×10^{-22}
Scheme B			
$CO_2 \rightarrow CO + O$	k_1[a]	1.89×10^{-4}	6.85×10^{-4}
$CO_2 + CH_4 \rightarrow CH_3COOH$	k_2[c]	2.07×10^{-22}	1.74×10^{-21}
$CH_4 \rightarrow CH_2 + H_2$	k_3[a]	1.48×10^{-4}	6.00×10^{-4}
$CH_3COOH + CH_2 \rightarrow RCOOH$	k_4[c]	1.37×10^{-22}	6.31×10^{-22}
$RCOOH \rightarrow CH_3COOH + CH_2$	k_5[a]	4.30×10^{-17}	4.82×10^{-17}
$CH_2 + H_2 \rightarrow CH_4$	k_6[c]	6.18×10^{-22}	1.41×10^{-22}
$CH_3COOH \rightarrow CO_2 + CH_4$	k_7[a]	3.16×10^{-4}	1.08×10^{-3}
$CO + O \rightarrow CO_2$	k_8[c]	1.42×10^{-20}	4.97×10^{-21}
$CO_2 + CH_4 \rightarrow X$	k_9[c]	4.27×10^{-23}	2.18×10^{-22}

Notes.
[a] Units in s^{-1} (first-order).
[b] RH = Hydrocarbons.
[c] Units in cm^2 $molecule^{-1}$ s^{-1} (second order).

few eV of kinetic energy (Bennett et al. 2006; Kim et al. 2010), which might be utilized to overcome the 106 kJ mol^{-1} (1.10 eV) entrance barrier (Bennett & Kaiser 2007) for the reaction of the hydrogen atom and carbon dioxide (CO_2) molecule to form trans-hydrocarboxyl radical (HOCO, Reaction (14)). The newly formed radicals (HOCO and R) may undergo barrier-less radical–radical recombination to form carboxylic acids (RCOOH), providing favorable geometry (Reaction (16)). Due to the facile conversion of this process (Kim & Kaiser 2010), the aforementioned mechanisms can be schematically streamlined to reactions (27) and (28) to be used in kinetic model A:

$$CH_4 \rightarrow RH, \quad (27)$$

$$RH + CO_2 \rightarrow RCOOH. \quad (28)$$

In addition, the destruction of carbon dioxide (CO_2) to carbon monoxide CO was considered in the reaction schemes:

$$CO_2 \rightarrow CO + O(^1D/^3P). \quad (29)$$

This reaction is endoergic by 532 kJ mol^{-1} (5.51 eV) for the triplet channel and by 732 kJ mol^{-1} (7.59 eV) for the singlet channel. The released suprathermal oxygen atoms may react back without an entrance barrier to recycle carbon dioxide (CO_2) (Bennett et al. 2011) or react with neighboring hydrocarbons to form alcohols (ROH) (Kaiser et al. 1999). Note that reasonable back reactions for reaction (27)–(29) were also added to the scheme (Kim & Kaiser 2010). The last reaction in Table 7 (rate constant k_7) accounts for additional miscellaneous reactions, which produce unknown species X.

Considering Scheme B, acetic acid (CH_3COOH) is considered the starting point of the formation of higher-order carboxylic acids. The formation of acetic acid was reported via reactions (12), (14), and (15) (Section 1), which can be streamlined to (Bennett & Kaiser 2007):

$$CH_4 + CO_2 \rightarrow CH_3COOH. \quad (30)$$

Then a successive insertion of suprathermal carbene (CH_2) might lead to the formation of higher-order carboxylic acids (RCOOH):

$$CH_3COOH + CH_2(a^1A_1) \rightarrow C_2H_5COOH, \quad (31)$$

$$C_2H_5COOH + CH_2(a^1A_1) \rightarrow i/n\text{–}C_3H_7COOH. \quad (32)$$

Back (rate constant k_5, k_6, k_7, and k_8) and miscellaneous reactions (rate constant k_9) were also considered in Scheme B. Note that the carbon-chain growth of the acids might also be due to radical–radical combination.

$$CH_3COOH \rightarrow CH_2COOH + H, \quad (33)$$

$$CH_2COOH + CH_3 \rightarrow C_2H_5COOH, \quad (34)$$

$$C_2H_5COOH \rightarrow C_2H_4COOH + H, \quad (35)$$

$$C_2H_4COOH + CH_3 \rightarrow i/n\text{–}C_3H_7COOH. \quad (36)$$

The simulations based on both schemes fit the temporal profiles (Figure 2). For Scheme A, irradiation at 5000 nA current caused faster decay of the carbon dioxide (CO_2, $k_1 = 6.41 \times 10^{-4}$ s^{-1}, $k_3 = 3.12 \times 10^{-19}$ cm^2 $molecule^{-1}$ s^{-1}, $k_7 = 2.06 \times 10^{-22}$ cm^2 $molecule^{-1}$ s^{-1}) and methane (CH_4, $k_2 = 8.71 \times 10^{-4}$ s^{-1}) than the 1000 nA current (carbon

dioxide (CO_2, $k_1 = 1.92 \times 10^{-4}$ s^{-1}, $k_3 = 3.26 \times 10^{-20}$ cm^2 $molecule^{-1}$ s^{-1}, $k_7 = 4.51 \times 10^{-23}$ cm^2 $molecule^{-1}$ s^{-1}) and methane (CH_4, $k_2 = 2.33 \times 10^{-4}$ s^{-1})) (Table 7). The formation of the products, carbon monoxide (CO) and carboxylic acids (RCOOH), were correspondingly faster during the high-dose irradiation. The simulations based on Scheme B gave comparable results. These data indicate that the formation of carboxylic acids follows the proposed reaction mechanisms involving a sequential mass growth process, which can proceed to scheme A and/or B.

5. Astrophysical Implications

The present study demonstrates the formation of high-order carboxylic acids ($C_nH_{2n+1}COOH$, n = 1–9) and determines the branching ratios of each acid in icy mixtures of carbon dioxide (CO_2) and methane (CH_4) (1:10) upon exposure to energetic electrons. Several previous studies also focused on producing carboxylic acids (RCOOH) in interstellar analogous ices. Only acetic acid (CH_3COOH) and possibly propionic acid (C_2H_5COOH) were identified in a low-dose radiolyzed carbon dioxide (CO_2) and methane (CH_4) ice (Bennett & Kaiser 2007). Another study of icy mixtures of carbon dioxide (CO_2) and hydrocarbon mixes (C_nH_{2n+2}, n = 1–6) reported the formation of higher-order carboxylic acids (RCOOH) (Kim & Kaiser 2010). However, the size and structure of the formed acids were not analyzed. In the present work, we monitored carboxylic acids from acetic acids (CH_3COOH) to decanoic acid ($C_9H_{19}COOH$) (Figures 3 and 4). The tentatively determined branching ratios of each acid were compiled in Table 6. Note that a higher radiation dose converts low-order acids such as acetic acid (CH_3COOH) and propionic acid (C_2H_5COOH) to higher-order carboxylic acids rather than decomposes/recycles large acids into small molecules.

In the ISM, although only formic acid (HCOOH) and acetic acid (CH_3COOH) have been detected, it is practical to anticipate the presence of higher-order carboxylic acids since the fractional abundances of the two observed acids decrease as the chemical complexity rises (Zuckerman et al. 1971; Liu et al. 2001; Remijan et al. 2002). Recently, the VIRTIS (Visible, Infrared, and Thermal Imaging Spectrometer) instrument on board the *Rosetta* spacecraft performed extensive spectral mapping of the surface of comet 67P/Churyumov–Gerasimenko and detected a broad absorption band centered at 3125 cm^{-1} (3.2 μm) (Quirico et al. 2016). The hydroxyl group in carboxylic acids (RCOOH) was suggested to be the most probable carrier since it is the sole candidate that encompasses the broad width of this absorption feature. Furthermore, the diversity of the carboxylic acids (RCOOH) characterized within our study (Figure 6) aligns closely with those identified in the meteorites (Figure 8). It is seen that the branching ratios of the acids are dissimilar in distinct meteorites (Figures 8(a) and (b)) (Lawless & Yuen 1979; Naraoka et al. 1999), which is possibly due to different parent bodies. Even for the same meteorite—Murchison—the ratios vary entirely upon different analytical methods (Figures 8(b) and (c)) (Lawless & Yuen 1979; Naraoka et al. 1999). The more recent and sensitive analysis (Figure 8(c)) shows that the ratio of branched carboxylic acids (RCOOH) to straight chain acids increases as the size of the acid increases (Huang et al. 2005). This result agrees quite well with our finding that most of the higher-order acids ($C_nH_{2n+1}COOH$, $n \geqslant 5$) detected in the current work are

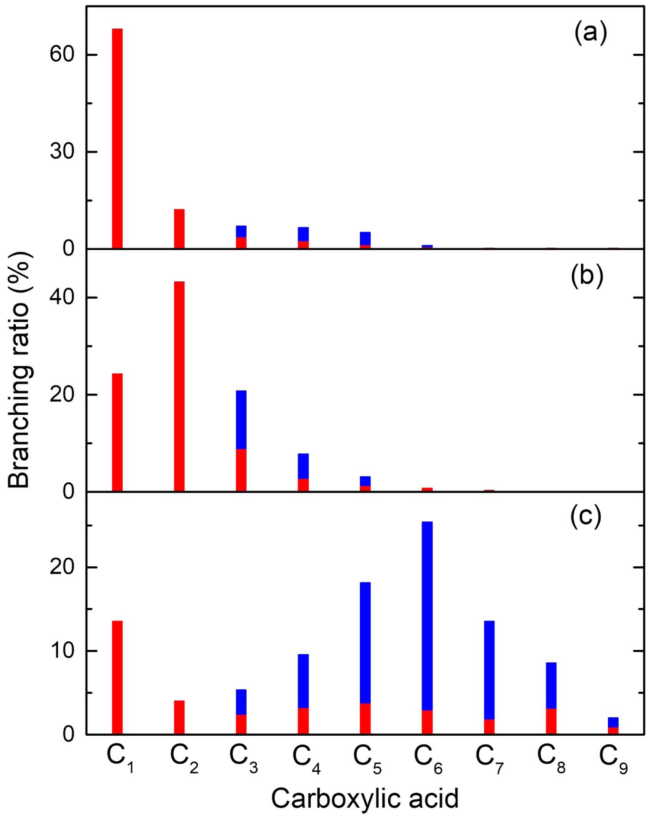

Figure 8. Branching ratios of the branched (blue rectangle) and straight (red rectangle) monocarboxylic acids ($C_nH_{2n-1}COOH$, n = 1–9) in: (a) A-881458 meteorite (Naraoka et al. 1999), (b) Murchison meteorite (Lawless & Yuen 1979), and (c) Murchison meteorite (Huang et al. 2005).

branched (Section 3.2). Limited by the current analysis method, the more detailed structural distribution of the acids cannot be unraveled. Further investigation using tunable photoionization coupled with reflectron time-of-flight mass spectrometry (PI-ReTOF-MS) might distinguish the isomers of the acids (Abplanalp et al. 2016b).

R.I.K. thanks the US National Science Foundation (AST-1505502) for its support. We thank Dr. Alexandre Bergantini and Sandor Gobi for advice regarding data processing.

ORCID iDs

Ralf I. Kaiser https://orcid.org/0000-0002-7233-7206

References

Abplanalp, M. J., Forstel, M., & Kaiser, R. I. 2016a, CPL, 644, 79
Abplanalp, M. J., Gozem, S., Krylov, A. I., et al. 2016b, PNAS, 113, 7727
Abplanalp, M. J., & Kaiser, R. I. 2016, ApJ, 827, 132
Abplanalp, M. J., & Kaiser, R. I. 2017, ApJ, 836, 195
Bennett, C. J., Hama, T., Kim, Y. S., Kawasaki, M., & Kaiser, R. I. 2011, ApJ, 727, 15
Bennett, C. J., Jamieson, C. S., Osamura, Y., & Kaiser, R. I. 2006, ApJ, 653, 792
Bennett, C. J., & Kaiser, R. I. 2007, ApJ, 660, 1289
Bertin, M., Romanzin, C., Michaut, X., Jeseck, P., & Fillion, J.-H. 2011, JPCC, 115, 12920
Bisschop, S., Jørgensen, J., van Dishoeck, E., & de Wachter, E. 2007, A&A, 465, 913
Boogert, A. A., Gerakines, P. A., & Whittet, D. C. 2015, ARA&A, 53, 541

Boonman, A. M. S., van Dishoeck, E. F., Lahuis, F., & Doty, S. D. 2003, A&A, 399, 1063
Bottinelli, S., Ceccarelli, C., Williams, J. P., & Lefloch, B. 2007, A&A, 463, 601
Bouilloud, M., Fray, N., Benilan, Y., et al. 2015, MNRAS, 451, 2145
Brunetto, R., Caniglia, G., Baratta, G., & Palumbo, M. 2008, ApJ, 686, 1480
Burke, D. J., Puletti, F., Woods, P. M., et al. 2015, JChPh, 143, 164704
Cazaux, S., Tielens, A. G. G. M., Ceccarelli, C., et al. 2003, ApJL, 593, L51
Center, R., & Mandl, A. 1972, JChPh, 57, 4104
Cernicharo, J., Marcelino, N., Roueff, E., et al. 2012, ApJ, 759, 43
d'Hendecourt, L., & Jourdain de Muizon, M. 1989, A&A, 223, L5
Donnay, J. D. H., & Ondik, H. M. 1972, Crystal Data: Determinative Tables, Vol. 1 (3rd ed.; Washington: NBS)
Drouin, D., Couture, A. R., Joly, D., et al. 2007, J. Scanning Micro, 29, 92
Ehrenfreund, P., Bernstein, M., Dworkin, J., Sandford, S., & Allamandola, L. 2001, ApJL, 550, L95
Ehrenfreund, P., & Charnley, S. B. 2000, ARA&A, 38, 427
Frenklach, M., Wang, H., & Rabinowitz, M. J. 1992, PrECS, 18, 47
Garrod, R., & Herbst, E. 2006, A&A, 457, 927
Garrod, R. T., Weaver, S. L. W., & Herbst, E. 2008, ApJ, 682, 283
Georgiou, C. D., & Deamer, D. W. 2014, AsBio, 14, 541
Gerakines, P. A., Bray, J. J., Davis, A., & Richey, C. R. 2005, ApJ, 620, 1140
Gerakines, P. A., Schutte, W. A., & Ehrenfreund, P. 1996, A&A, 312, 289
Gerakines, P. A., Schutte, W. A., Greenberg, J. M., & Vandishoeck, E. F. 1995, A&A, 296, 810
Gibb, E. L., Whittet, D. C. B., Boogert, A. C. A., & Tielens, A. G. G. M. 2004, ApJS, 151, 35
Goumans, T., Uppal, M. A., & Brown, W. A. 2008, MNRAS, 384, 1158
Gross, J. H. 2004, Mass Spectrometry-A Textbook (1st ed.; Heidelberg: Springer)
Huang, Y., Wang, Y., Alexandre, M. R., et al. 2005, GeCoA, 69, 1073
Ikeda, M., Ohishi, M., Nummelin, A., et al. 2001, ApJ, 560, 792
Irvine, W. M., Friberg, P., Kaifu, N., et al. 1989, A&A, 229, L9
Irvine, W. M., Friberg, P., Kaifu, N., et al. 1990, A&A, 229, L9
Jamieson, C. S., Mebel, A. M., & Kaiser, R. I. 2006, ApJS, 163, 184
Jones, B. M., & Kaiser, R. I. 2013, JPCL, 4, 1965
Jørgensen, J. K., van der Wiel, M. H. D., Coutens, A., et al. 2016, A&A, 595, A117
Kaiser, R., & Suits, A. G. 1995, RScI, 66, 5405
Kaiser, R. I., Eich, G., Gabrysch, A., & Roessler, K. 1999, A&A, 346, 340
Kaiser, R. I., Gabrysch, A., & Roessler, K. 1995, RScI, 66, 3058
Kaiser, R. I., & Roessler, K. 1998, ApJ, 503, 959
Keane, J. V., Tielens, A. G. G. M., Boogert, A. C. A., Schutte, W. A., & Whittet, D. C. B. 2001, A&A, 376, 254
Kim, Y., Bennett, C., Chen, L.-H., O'Brien, K., & Kaiser, R. I. 2010, ApJ, 711, 744
Kim, Y., & Kaiser, R. I. 2010, ApJ, 725, 1002
Lacy, J., Carr, J., Evans, N. J., et al. 1991, ApJ, 376, 556
Lawless, J. G., & Yuen, G. U. 1979, Natur, 282, 396
Liu, S.-Y., Mehringer, D. M., & Snyder, L. E. 2001, ApJ, 552, 654
Martins, Z., Watson, J., Sephton, M., et al. 2006, M&PS, 41, 1073
McDonald, G. D., Whited, L. J., DeRuiter, C., et al. 1996, Icar, 122, 107
McLafferty, F. W. 1959, AnaCh, 31, 82
McMurtry, B. M., Saito, S. E., Turner, A. M., Chakravarty, H. K., & Kaiser, R. I. 2016, ApJ, 831, 174
Mebel, A. M., Lin, S.-H., & Chang, C.-H. 1997, JChPh, 106, 2612
Mehringer, D. M., Snyder, L. E., Miao, Y., & Lovas, F. J. 1997, ApJL, 480, L71
Monroe, A. A., & Pizzarello, S. 2011, GeCoA, 75, 7585
Naraoka, H., Shimoyama, A., & Harada, K. 1999, OLEB, 29, 187
Öberg, K. I., Boogert, A. A., Pontoppidan, K. M., et al. 2008, ApJ, 678, 1032
Palau, A., Walsh, C., Sanchez-Monge, A., et al. 2017, MNRAS, 467, 2723
Pittam, D., & Pilcher, G. 1972, FaTr, 68, 2224
Pizzarello, S., Huang, Y., Becker, L., et al. 2001, Sci, 293, 2236
Pizzarello, S., Huang, Y., & Fuller, M. 2004, GeCoA, 68, 4963
Pontoppidan, K. M., Boogert, A. C., Fraser, H. J., et al. 2008, ApJ, 678, 1005
Quirico, E., Moroz, L., Schmitt, B., et al. 2016, Icar, 272, 32
Remijan, A., Snyder, L. E., Friedel, D. N., Liu, S.-Y., & Shah, R. Y. 2003, ApJ, 590, 314
Remijan, A., Snyder, L. E., Liu, S.-Y., Mehringer, D., & Kuan, Y.-J. 2002, ApJ, 576, 264
Requena-Torres, M. A., Marcelino, N., Jiménez-Serra, I., et al. 2007, ApJL, 655, L37
Requena-Torres, M. A., Martín-Pintado, J., Rodríguez-Franco, A., et al. 2006, A&A, 455, 971
Sander, W., & Gantenberg, M. 2005, AcSpA, 62, 902
Schutte, W. A., Boogert, A. C. A., Tielens, A., et al. 1999, A&A, 343, 966
Shiao, Y.-S. J., Looney, L. W., Remijan, A. J., Snyder, L. E., & Friedel, D. N. 2010, ApJ, 716, 286
Smith, K. E., Gerakines, P. A., & Callahan, M. P. 2015, ChCom, 51, 11787
Socrates, G. 2004, Infrared and Raman Characteristic Group Frequencies (3rd ed.; New York: Wiley)
Sugimura, M., Yamaguchi, T., Sakai, T., et al. 2011, PASJ, 63, 459
Tsang, W. 1996, HeStructure Energetics and Reactivity in Chemistry Vol. 4 (Berlin: Springer)
Turner, A. M., Abplanalp, M. J., Chen, S. Y., et al. 2015, PCCP, 17, 27281
Vinogradoff, V., Le Guillou, C., Bernard, S., et al. 2017, GeCoA, 212, 234
Wyckoff, R. 1965, Crystal Structures, Vol. 4 (New York: Wiley)
Yuen, G. U., & Kvenvolden, K. A. 1973, Natur, 246, 301
Zhou, L., Maity, S., Abplanalp, M., Turner, A., & Kaiser, R. I. 2014, ApJ, 790, 38
Zuckerman, B., Ball, J. A., & Gottlieb, C. A. 1971, ApJL, 163, L41